Compound material point method (CMPM) to improve stress recovery for quasi-static problems

Gonzalez Acosta, Leon; Vardon, Phil; Hicks, Michael

DOI
10.1016/j.proeng.2017.01.037

Publication date
2017

Document Version
Final published version

Published in
Procedia Engineering

Available online at www.sciencedirect.com

ScienceDirect

Procedia Engineering 175 (2017) 324 – 331

Procedia Engineering

www.elsevier.com/locate/procedia

1st International Conference on the Material Point Method, MPM 2017

Composite material point method (CMPM) to improve stress recovery for quasi-static problems

Leon Gonzalez Acosta[a], Phil J. Vardon[a,*], Michael A. Hicks[a]

[a]*Geo-Engineering Section, Delft University of Technology, Delft, The Netherlands*

Abstract

Stress oscillations and inaccuracies are commonly reported in the material point method (MPM). This paper investigates the causes and presents a method to reduce them. The oscillations are shown to result from, at least in part, two distinctly different causes, both originating from the shape function approximations used. The first is due to the components of the stiffness matrix (or other matrices) being derived by performing numerical integration using the material points, and the second is due to calculating the strain from the nodal displacements of the elements, interpolated to the material points, via the shape function spatial derivatives. In this paper, an improvement for the recovery of results from the nodes to the material points is presented, where an increase of the C^n continuity along with an interpolation involving nodes from neighbouring elements is applied.

Peer-review under responsibility of the organizing committee of the 1st International Conference on the Material Point Method

Keywords: material point method; particle-in-cell; shape functions; stress oscillation; stress recovery.

1. Introduction

The material point method (MPM) has proven to be a useful numerical technique for solving problems involving large deformations. Recently, several attempts have been made to demonstrate the effectiveness of MPM for geotechnical applications. For example, Wang et al. [1-3] and Llano-Sema et al. [4] have successfully computed landslide mechanisms using MPM, Beuth et al. [5] solved a retaining wall problem, and Andersen and Andersen [6] modelled the collapse of a soil column. These previous numerical examples have computed typical soil behaviour,

* Corresponding author.
E-mail address: p.j.vardon@tudelft.nl

Peer-review under responsibility of the organizing committee of the 1st International Conference on the Material Point Method
doi:10.1016/j.proeng.2017.01.037

albeit using relatively simple constitutive models, in particular with respect to shear failure. However, stress oscillations have been observed [e.g. 4]. To utilize more complex constitutive behaviour typical of soils, e.g. stress dependency, dilatancy, non-linearity and stress history dependency, a consistent and reliable stress determination is imperative.

A number of approaches for smoothing the shape function discontinuities between elements have been proposed, including the generalized interpolation material point method (GIMPM) by Bardenhagen and Kober [7] and convected particle domain interpolation (CPDI) by Sadeghirad et al. [8].

This paper proposes another method, the composite material point method (CMPM), that reduces stress oscillations by improving the stress recovery procedure based on the composite finite element method (CFEM) of Sadeghirad and Astaneh [9]. CMPM increases the C^n ($n \geq 0$) continuity to smooth the solution and reduce discontinuities along inter-element boundaries, by considering linear and high-order quadrilateral elements. Initially, a brief demonstration of the causes of the stress oscillations is made, followed by an overview of the proposed CMPM formulation and a simple example to demonstrate its applicability.

2. Stress oscillations

An illustration of stress oscillations caused in MPM is presented in this section. This involves the analysis of a thick-walled cylinder subjected to an internal pressure, as shown in Fig. 1. An internal radial displacement is applied at the inner boundary ($r = r_i$) and the outer boundary is fixed ($r = r_e$). An axisymmetric geometry is used, with either 4 or 8 noded quadrilateral elements.

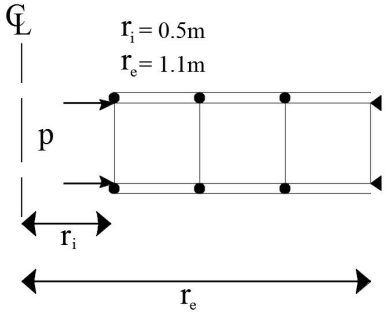

Fig. 1. Thick-walled cylinder under internal pressure.

The displacement has been applied in a single step and the incremental stress change determined across the whole domain. The material points are initially located at the Gauss point locations and, therefore, for the stiffness matrix calculation, it is the same as for FEM.

Fig. 2 shows that, depending on the element type and the value of the Poisson ratio, the stress distribution takes on different shapes and magnitudes. For linear elements (Fig. 2a), the stress distribution within the element is almost linear, while high order elements show a second order stress distribution (Fig. 2b). It is also evident that stress oscillations for linear elements are greater than for high order elements, especially close to the external boundaries. Different examples for stress oscillations and stress paths can be found in the literature, as in Yerro et al. [10], where *p-q* stress paths are plotted for a slope stability problem.

In Fig. 2, the stress is observed to be continuous within each element and discontinuous across elements. It is also noted that the stress solution is almost exact at the centres of the linear elements and at the reduced Gauss point locations in the quadratic elements, as has been noted by others; most notably, by Naylor [11] and Mar and Hicks [12], who analyzed a similar thick-walled cylinder problem to investigate stress oscillation and possible mitigation mesures in FEM. In an MPM simulation with multiple load/displacement steps, stress oscillations will occur due to both the shape function characteristics and material points crossing inter-element boundaries, where shape functions are no longer continuous.

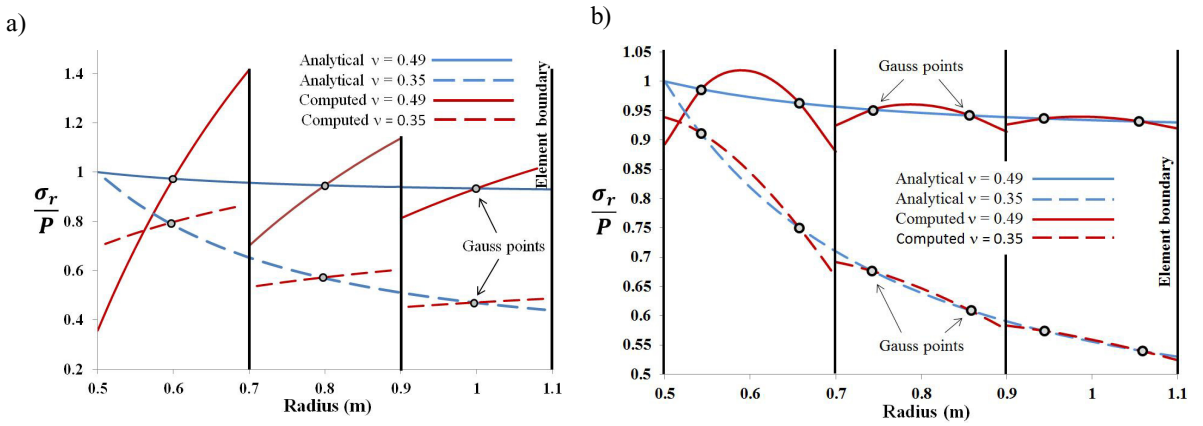

Fig. 2. Stress oscillation considering (a) 4 noded elements and (b) 8 noded elements.

3. CMPM theoretical aspects

The basis of CMPM, as in other MPM methods, is that the original FEM shape functions are utilised for the formation of the stiffness matrices. Hence, the CFEM method [9] has been integrated into an MPM code. A quasi-static version of MPM [1] has been used here to demonstrate the behaviour, although this approach can also be directly used in dynamic versions [e.g. 1-3].

3.1. Shape functions for 2D linear (4-noded) quadrilateral base elements

The objective of CMPM is to increase the stress recovery precision, by increasing the solution domain for each element through considering values of neighbouring nodes in the grid. Due to the increase in size of the solution domain, higher order shape functions are used, since more nodes are included in the shape function interpolations, with the new order being directly related to the order of the continuity C^n and the relative position of the element. Fig. 3 demonstrates the nature of the shape functions for element *J*, with C^1 continuity, for a boundary element and a middle element. In the case of a boundary element (Fig. 3a), C^1 continuity can be applied to only one side of the element, since only on this side are there nodes to interpolate the solution, and this leads to the use of quadratic shape functions. In contrast, in the case of a middle element (Fig. 3b), C^1 continuity is applied to both sides of the element, increasing the order of the shape functions to three.

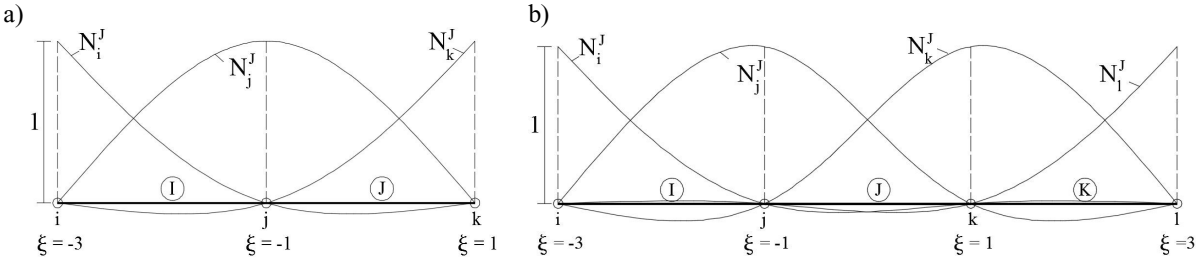

Fig. 3. 1D element shape functions considering (a) one neighbouring node and (b) two neighbouring nodes.

In Fig. 3, N are the shape functions, ξ is the local coordinate, *i, j, k* and *l* are the node numbering, I, J and K are the elements, and the subscripts and superscripts are related with the node and element for which the shape functions are computed, respectively. With reference to Fig. 3a, for the boundary element J, with only one neighbouring node i in element I, the shape functions are computed as:

$$\begin{bmatrix} N_i^J \\ N_j^J \\ N_k^J \end{bmatrix} = \begin{bmatrix} \frac{-1}{8}(1-\xi)(1+\xi) \\ \frac{1}{4}(1-\xi)(3+\xi) \\ \frac{1}{8}(1+\xi)(3+\xi) \end{bmatrix} \tag{1}$$

For the middle element J (Fig. 3b), the shape functions with C^1 continuity are computed as:

$$\begin{bmatrix} N_i^J \\ N_j^J \\ N_k^J \\ N_l^J \end{bmatrix} = \frac{1}{16}\begin{bmatrix} (1-\xi)(1+\xi)^2 \\ (1-\xi)(9-2\xi-3\xi) \\ (1+\xi)(9+2\xi-3\xi) \\ (1+\xi)(1-\xi)^2 \end{bmatrix} \tag{2}$$

In the case of 2D elements (Fig. 4), the same rules are applied for the development of the shape functions, with the new shape functions being formed by the multiplication of the previous 1D shape functions. Hence, the shape functions for the boundary element E4 (Fig. 4a), and for the middle element E5 (Fig. 4b), are as follows:

$$N_{n\alpha\beta}^{E1}\left(\xi^{E1},\eta^{E1}\right) = N_{n\alpha}^{E1}\left(\xi^{E1}\right)N_{n\beta}^{E1}\left(\eta^{E1}\right) \qquad \begin{cases} \alpha = 1,2,3 \\ \beta = 1,2,3 \end{cases} \tag{3}$$

$$N_{n\alpha\beta}^{E5}\left(\xi^{E5},\eta^{E5}\right) = N_{n\alpha}^{E5}\left(\xi^{E5}\right)N_{n\beta}^{E5}\left(\eta^{E5}\right) \qquad \begin{cases} \alpha = 1,2,3,4 \\ \beta = 1,2,3,4 \end{cases} \tag{4}$$

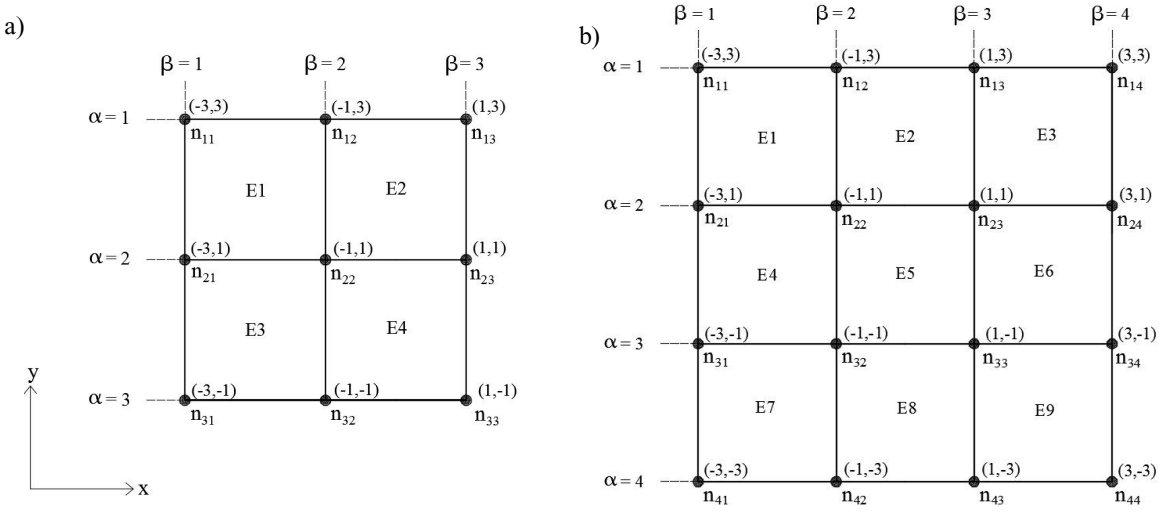

Fig. 4. Solution domain for C^1 continuity for (a) boundary element E4 and (b) middle element E5.

A detailed explanation on how to create 1D and 2D element shape functions with C^n ($n \geq 1$) continuity, along with Kronecker-delta and partition of unity properties, can be found in [7].

3.2. Shape functions for 2D quadratic (8-noded) quadrilateral base elements

For 2D 8-noded quadrilateral elements, the domain is increased by considering only 3 neighbour elements. In this case, the shape functions for domain Ω, where $\Omega = E_1 + E_2 + E_3 + E_4$ (Fig. 5), can be computed by taking the equations for quadratic serendipity elements from Oñate [13] as follows:

$$N(\xi,\eta) = \begin{cases} \frac{1}{12}(1+\xi\xi_i)(1+\eta\eta_i)\left[4(\xi^2-1)\xi\xi_i + 4(\eta^2-1)\eta\eta_i + 3\xi\eta\xi_i\eta_i\right] & \xi_i = \pm 1,\ \eta_i = \pm 1 \\ 2(1+\xi\xi_i)(\eta^2-1)(\eta^2-\xi\xi_i/4) & \xi_i = \pm 1,\ \eta_i = 0 \\ 2(1+\eta\eta_i)(\xi^2-1)(\xi^2-\eta\eta_i/4) & \xi_i = 0,\ \eta_i = \pm 1 \\ \frac{4}{3}(1+\xi\xi_i)(1-\eta^2)(\eta^2+\eta\eta_i) & \xi_i = \pm 1,\ \eta_i = \pm\frac{1}{2} \\ \frac{4}{3}(1+\eta\eta_i)(1-\xi^2)(\xi^2+\xi\xi_i) & \xi_i = \pm\frac{1}{2},\ \eta_i = \pm 1 \\ (1-\xi^2)(1-\eta^2) & \xi_i = 0,\ \eta_i = 0 \end{cases} \tag{5}$$

where ξ_i and η_i correspond to the local coordinates of the nodes in Ω.

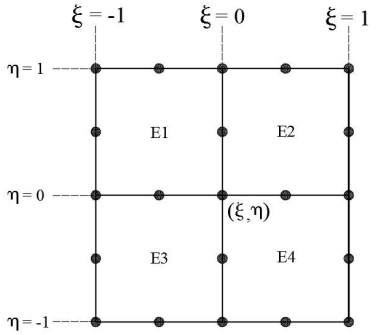

Fig. 5. Solution domain for stress recovery with high-order square elements with CMPM.

4. CMPM implementation

4.1. Stress recovery

To increase the accuracy of the stress recovery procedure by using CMPM, a loop over each material point can be performed over each sub-region (Fig. 6), where, for 8 node elements, each sub-region is the union of 1 element containing materials points with 3 neighbouring elements (as mentioned above). However, note that in the case of C^1 continuity for a 4 node middle element (as in Fig. 4b), sub-regions are not necessary. Next, the strain interpolation in the case of C^1 continuity can be computed as:

$$\Delta\boldsymbol{\varepsilon}(\boldsymbol{x}_p) = \frac{1}{S}\sum_{i=1}^{S}\boldsymbol{B}(\boldsymbol{x}_p)\Delta\boldsymbol{a} \tag{6}$$

where $\Delta\boldsymbol{\varepsilon}$ is the strain increment vector, S is the number of sub-regions, $\boldsymbol{B}$ is the strain-displacement matrix, $\Delta\boldsymbol{a}$ is the vector of incremental displacements for each sub-region and $\boldsymbol{x}_p$ is the position of the material point. Finally, the stresses $\Delta\boldsymbol{\sigma}$, which are a function of the material point position $\boldsymbol{x}_p$, can be computed using the material stiffness matrix $\boldsymbol{D}^e$ as:

$$\Delta\boldsymbol{\sigma}(\boldsymbol{x}_p) = \boldsymbol{D}^e \Delta\boldsymbol{\varepsilon}(\boldsymbol{x}_p) \tag{7}$$

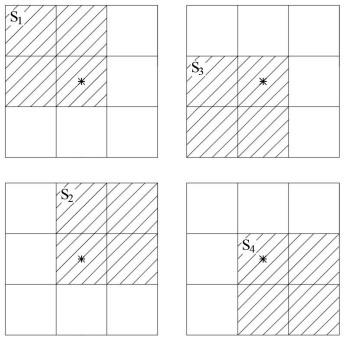

Fig. 6. Sub-regions for stress recovery at a middle material point.

4.2. Numerical example of an internally displaced cylinder

To demonstrate the accuracy of CMPM compared with regular MPM, the radial stress distribution through the wall of a cylinder fixed at the outer boundary and subjected to a prescribed radial displacement at the inner boundary is investigated, considering both constant (labelled "kconst") and non-constant (labelled "knon") element stiffness matrices. An axisymmetric analysis is carried out, with the 2D elements representing a cross-section through the cylinder wall. The domain is discretized by 9 elements from, r_i = 0.5 m to r_e = 1.1 m, with 4 material points per element initially located at the Gauss points position (Fig. 7). The cylinder is assumed to be linear elastic, with $E = 2500\ kN$ and $\nu = 0.35$ or $\nu = 0.49$. The pressure at the internal boundary is applied by prescribing 2 cm increments of radial displacement.

Two versions of the code are used, to separate the impact of the stiffness matrix determination and the stress recovery. The first version of the code uses a constant (i.e. fixed) stiffness matrix per finite element, which is determined only once at the start of the analysis. The second uses a constant stiffness per material point, with the nodal values in the stiffness matrix changing based on the numerical integration.

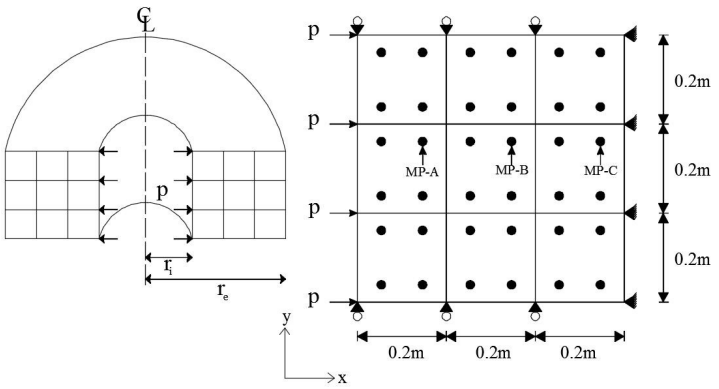

Fig. 7. Internal radial displacement of a cylinder fixed at the outer boundary.

4.3. Results

The results obtained from the analysis with 4 noded elements are shown in Fig. 8. As can be seen, in Fig. 8a, considering $\nu = 0.35$, the stresses oscillate around the analytical solution due to the sub-optimal positions at which stresses are being evaluated (Gauss quadrature rule not satisfied), this causing a lack of accuracy in the stress recovery. Also, the results for the material points in boundary elements are less accurate than those for the middle element, due to the boundary elements having less information from neighbouring elements than the middle element. Fig. 8b shows similar findings for $\nu = 0.49$, although the oscillations are now larger due to the near incompressibility of the cylinder wall. After step 4, the stress computed for material point MP-A using regular MPM suffers an abrupt change after crossing an element boundary (Fig. 9), due to the lack of continuity in the shape functions. In contrast, the computed stresses using CMPM are smoother before, during and after element crossing. It is also important to note that, due to CMPM gathering information from neighbouring elements, if the nodal values of these elements are carrying wrong values, this will contribute to a wrong evaluation of the strains and stresses at the material points.

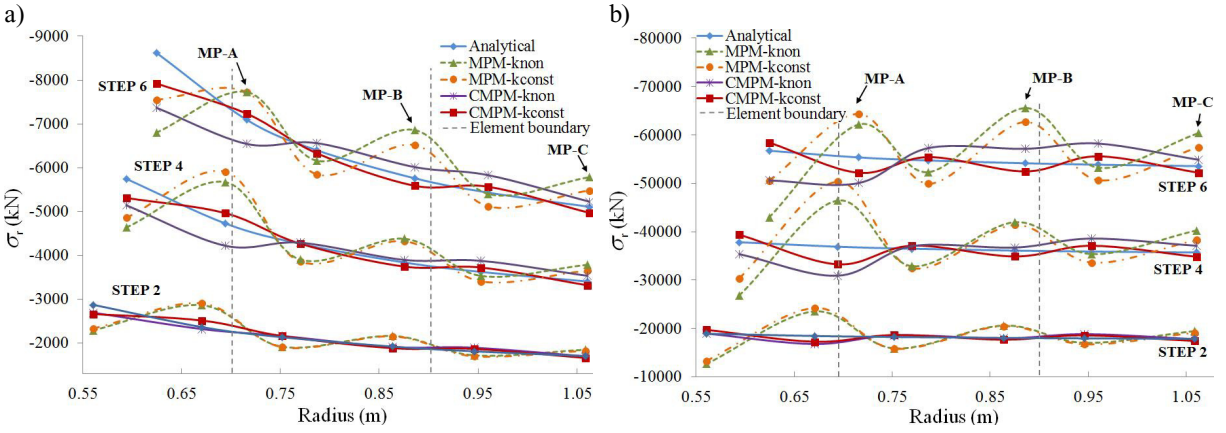

Fig. 8. Comparison of radial stress distributions with 4-noded elements and (a) $\nu = 0.35$, and (b) $\nu = 0.49$.

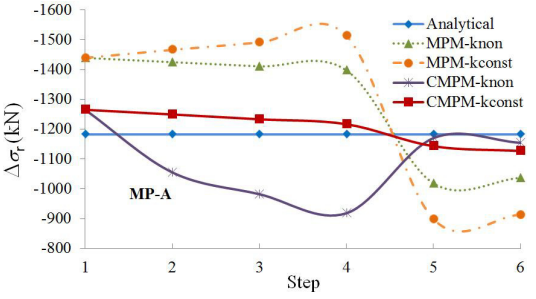

Fig. 9. Incremental radial stresses at material point MP-A for each step considering $\nu = 0.35$.

Finally, Fig. 10 shows the radial stress σ_r after steps 1, 3 and 5, when using 8-noded square elements and $\nu = 0.35$. By comparing the results for regular MPM with constant stiffness (i.e. MPM-kconst) and CMPM-kconst, it can be seen that the stress oscillation is small and almost the same in both cases (Fig. 10a), and that the change in stress after element crossing (Fig. 10b) is not as big as in the 4-node analysis. This shows that, for 8 node elements, the stress recovery procedure can be accurate even for regular MPM. The main problem is related with the stiffness matrix, as can be seen from both the MPM-knon and CMPM-knon results, where the increase in oscillation comes from an inaccurate stiffness matrix evaluation.

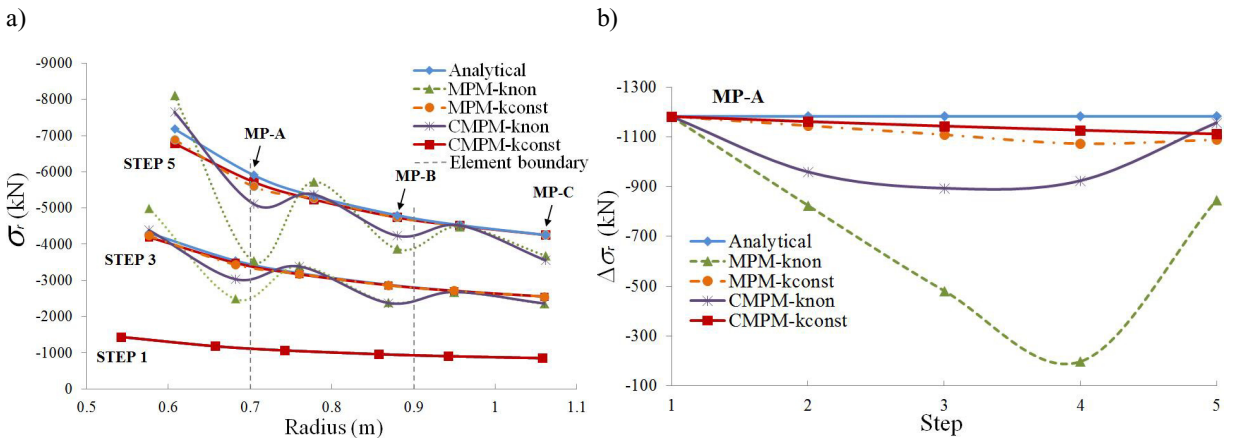

Fig. 10. (a) Comparison of radial stress distributions with 8-noded elements after steps 1, 3 and 5, and (b) incremental radial stresses at material point MP-A for each step.

5. Conclusion

This paper has shown that the classical MPM stress recovery procedure can be improved with CMPM, which increases the accuracy of the results by increasing the size of the interpolation domain. By comparing the results for 4 noded elements with those for 8 noded elements, CMPM shows an improved performance for 4 noded elements, whereas the stress behaviour for 8 noded elements can be drastically improved, for both MPM and CMPM, with only the correct evaluation of the stiffness matrix (kconst) for every time step. This is because the rate of oscillation is always higher for 4 noded elements, independent of the material properties. It is also evident that the CMPM solutions for both element types are still close to the analytical solution after crossing element boundaries. This allows for an accurate stress history to be maintained, which is crucial for history-dependent materials. Finally, special attention has to be paid to 8 noded elements during stiffness matrix evaluation, since poor evaluation of the stiffness matrix can cause severe changes to the calculated nodal displacement values.

References

[1] Wang B, Vardon PJ, Hicks MA, Chen Z. Development of an implicit material point method for geotechnical applications. Comput Geotech 2016;71:159-67.
[2] Wang B, Vardon PJ, Hicks MA. Investigation of retrogressive and progressive slope failure mechanisms using the material point method. Comput Geotech 2016;78:88-98.
[3] Wang B, Hicks MA, Vardon PJ. Slope failure analysis using the random material point method. Géotechnique Letters 2016;6(2):113-18.
[4] Llano-Sema MA, Farias MM, Pedroso DM. An assessment of the material point method for modelling large scale run-out processes in landslides. Landslides 2015. http://dx.doi.org/10.1007/s10346-015-0664-4
[5] Beuth L, Więckowski Z, Vermeer PA. Solution of quasi-static large-strain problems by material point method. Int J Numer Anal Meth Geomech 2010;35:1451-65.
[6] Andersen S, Andersen L. Analysis of stress updates in the material-point method. The Nordic Seminar on Computational Mechanics 2009;11:129-34.
[7] Bardenhagen SG, Kober EM. The generalized interpolation material point method. Comput Model Eng Sci 2004;5(6):477-96.
[8] Sadeghirad A, Brannon RM, Burghardt J. A convected particle domain interpolation technique to extend applicability of the material point method for problems involving massive deformations. Int J Numer Meth Eng 2011;86:1435-56.
[9] Sadeghirad A, Astaneh AV. A finite element method with composite shape functions. Engineering Computations: International journal of computer-aided engineering and software 2011;28:389-422.
[10] Yerro A, Alonso EE, Pinyol NM. The material point method for unsaturated soils. Géotechnique 2015;65(3):201-217.
[11] Naylor DJ. Stresses in nearly incompressible materials by finite elements with application to the calculation of excess pore pressure. Int J Numer Meth Eng 1974;8:443-60.
[12] Mar A, Hicks MA. A benchmark computational study of finite element error estimation. Int J Numer Meth Eng 1996;39:3969-83.
[13] Oñate E. Struct*ural analysis with the finite element method*. Barcelona, Spain. Artes Gráficas Torres S.L.; 2009.